Electric Field Induced Alignment of Concentrated Block Copolymer Solutions

A. Böker,[†,‡,^] H. Elbs,[†] H. Hänsel,[†] A. Knoll,[†] S. Ludwigs,[†] H. Zettl,[†] A. V. Zvelindovsky,[⊥] G. J. A. Sevink,[⊥] V. Urban,[#,▽] V. Abetz,[‡] A. H. E. Müller,[‡,§] and G. Krausch*[,†,§]

Lehrstuhl für Physikalische Chemie II, Lehrstuhl für Makromolekulare Chemie II, and Bayreuther Zentrum für Kolloide und Grenzflächen, Universität Bayreuth, D-95440 Bayreuth, Germany; Universiteit Leiden, LIC, P.O. Box 9502, 2300 RA Leiden, The Netherlands; and European Synchrotron Radiation Facility (ESRF), F-38043 Grenoble, France

Received August 19, 2002

ABSTRACT: We investigate the microdomain orientation kinetics of concentrated block copolymer solutions exposed to a dc electric field by time-resolved synchrotron small-angle X-ray scattering. As a model system, we use a lamellar polystyrene-*b*-polyisoprene block copolymer dissolved in toluene. Our results indicate two different microscopic mechanisms, i.e., nucleation and growth of domains and grain rotation. The former dominates close to the order−disorder transition, while the latter prevails under more strongly segregated conditions. This conclusion is corroborated by computer simulations based on dynamic density functional theory. The orientation kinetics follows a single-exponential behavior with characteristic time constants varying from a few seconds to some minutes depending on polymer concentration, temperature, and electric field strength. From the experimental results we deduce optimum conditions for the preparation of highly anisotropic bulk polymer samples via solvent casting in the presence of an electric field.

Introduction

Block copolymers composed of incompatible components self-assemble into microphase-separated domains usually leading to well-ordered structures on the mesoscale.[1,2] However, in the absence of external fields, typically an isotropic grain structure is obtained characterized by a random distribution of microdomain orientations. It is well-known from thin-film studies that external interfaces can align the block copolymer morphology, given that the interface selectively attracts one of the constituent blocks.[3,4] Usually, however, the influence of the substrate on the alignment decays quite rapidly with the distance; i.e., after several long periods a more or less random orientation is observed as it is typical for the bulk state. To achieve large-scale alignment throughout a macroscopically extended bulk sample, different techniques have been devised in the past. Most prominently, external mechanical fields have been successfully applied to orient block copolymer melts and solutions, e.g., large-amplitude oscillatory shear (LAOS)[5−7], extrusion,[8] or roll-casting.[9]

In addition to mechanical fields, the potential of electric fields for microdomain alignment has attracted increasing interest in the recent past as it may also have a considerable technological potential.[10] It has been shown that both lamellar and cylindrical microdomain structures in polystyrene-*b*-poly(methyl methacrylate) (PS-*b*-PMMA) thin films could be oriented by virtue of a dc electric field.[11−17] These melt-based electric field procedures suffer from severe limitations due to the high melt viscosities typical for high molecular weight copolymers or copolymers of more complex architectures and the chemical instability at high temperatures. To overcome these limitations, one can try to align concentrated block copolymer solutions, where a nonselective solvent is used to induce sufficient mobility. Following earlier investigations by Le Meur et al.,[18] we recently investigated the microdomain alignment of an ABC triblock copolymer during solvent casting in the presence of an external dc electric field.[19] After drying, bulk samples of the material exhibited lamellar microdomains highly oriented parallel to the electric field vector, as shown by small-angle X-ray scattering (SAXS) and transmission electron microscopy (TEM).

In the present paper, we describe real-time synchrotron radiation small-angle X-ray scattering (synchrotron SAXS) investigations aiming to follow the kinetics of electric-field-induced microdomain reorientation in concentrated block copolymer solutions and, thus, to elucidate the underlying microscopic mechanisms. As a model system, we investigate the orientation behavior of a lamellae-forming polystyrene-*b*-polyisoprene diblock copolymer dissolved in toluene. We discuss the influence of the polymer concentration, the electric field strength, and the temperature on the reorientation behavior. We identify two different microscopic processes, nucleation and growth of domains and grain rotation, which are found to dominate the reorientation process in different regimes of block copolymer concentration and temperature. Part of this work has recently been published.[20]

[†] Lehrstuhl für Physikalische Chemie II, Universität Bayreuth.
[‡] Lehrstuhl für Makromolekulare Chemie II, Universität Bayreuth.
[§] Bayreuther Zentrum für Kolloide und Grenzflächen, Universität Bayreuth.
[⊥] Universiteit Leiden.
[#] European Synchrotron Radiation Facility.
[^] Present address: Department of Polymer Science and Engineering, University of Massachusetts, Amherst, MA 01003, USA.
[▽] Present address: Oak Ridge National Laboratory (ORNL), Oak Ridge, TN 37831, USA.
* Corresponding author. E-mail: georg.krausch@uni-bayreuth.de.

10.1021/ma021347k CCC: $25.00
Published on Web 09/18/2003

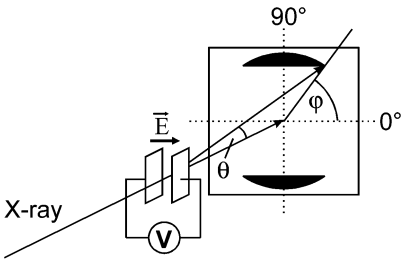

Figure 1. Experimental setup for in-situ SAXS.

In addition to the experiments, we performed computer simulations based on dynamic density functional theory (DDFT).[21]

The paper is organized as follows. In the Methods section we describe experimental and simulation techniques. In the Results and Discussion section we shall first describe the structure formation in solution and its properties before we continue discussing the influence of an external electric field on the domain orientation of solutions of different concentrations, at different electric field strengths, and at different temperatures. We compare the experimental results with computer simulations using dynamic density functional theory. We will end the discussion by showing how our results can be used to generate well-aligned block copolymer bulk samples.

Methods

Synthesis. A polystyrene-*b*-polyisoprene block copolymer (SI-80) with a total number-average molecular weight M_n = 80 kg/mol was synthesized by sequential living anionic polymerization as described in detail elsewhere.[22] The polymer used in this study consists of 52 wt % polystyrene and 48 wt % polyisoprene (92% 1,4-cis, 4% 1,2, and 4% 3,4 microstructure). Gel permeation chromatography (GPC) of the final block copolymer yields a polydispersity M_w/M_n = 1.02. The block ratio and overall molecular weight were determined by ^{1}H NMR using the integrated aromatic signals of the polystyrene block in combination with the GPC results of the corresponding polystyrene precursor.

Sample Preparation. Toluene solutions of the block copolymer with concentrations ranging from 30 to 80 wt % were prepared. The alignment experiments were performed in a home-built capacitor with gold electrodes (sample depth = 5 mm, electrode distance d = 2 mm) at temperatures ranging from room temperature up to 80 °C. A dc voltage between 0.5 and 6 kV was applied across the capacitor, resulting in a homogeneous electric field pointing perpendicular to the X-ray beam direction (Figure 1). Both the voltage at the electrodes and the current through the sample were monitored during the course of the experiment. Within the sensitivity of the setup ($I \approx 0.01$ mA), no leakage currents were detected after the electric field was applied. The sample temperature was controlled to within ±1 °C using Peltier elements.

Synchrotron Small-Angle X-ray Scattering (Synchrotron SAXS). Synchrotron SAXS measurements were performed at the ID02 beamline at the European Synchrotron Radiation Facility (ESRF, Grenoble, France). The typical photon flux routinely obtained at the ID02 sample position is 10^{13} photons/s at an energy width $\Delta E/E = 2 \times 10^{-4}$. The operating beam energy was 12.5 keV, corresponding to a peak wavelength of 0.1 nm. The beam direction (cross section: 200 × 200 μm^2) was perpendicular to the direction of the applied electric field.

The detector system is housed in a 10 m evacuated flight tube. An image intensified CCD detector was used, which can handle the full X-ray flux. The CCD is capable of acquiring up to 10 frames of 1024 × 1024 pixels/s, and a sequence of up to 125 frames can be acquired with this time resolution. Prior to data analysis, background scattering was subtracted from the data, and corrections were made for spatial distortions and for the detector efficiency.

Transmission Electron Microscopy (TEM). Some of the samples were dried in the presence of the electric field. Subsequently, thin sections were cut parallel to the electric field vector (far from any surface) using a Reichert-Jung Ultracut E microtome equipped with a diamond knife. To enhance the electron density contrast between polystyrene and polyisoprene, the sections were exposed to RuO_4 vapor for 45 min, which leads to a preferential staining of the polystyrene block.[23] Bright field TEM was performed using a Zeiss electron microscope (CEM 902) operated at 80 kV.

Calculation of Order Parameters. As will become clear from the experimental observations described below, domain alignment is induced by two competing external fields of different symmetry, i.e., namely the interfacial field between polymer solution and the electrode surfaces and the external electric field. To quantify the microdomain alignment, we calculate the order parameter P_2 by integrating the scattering intensity $I_q(\varphi)$ over the azimuthal angle φ from $\varphi = 0°$ to 360°:

$$P_2 = \frac{3\langle\cos^2\varphi\rangle - 1}{2} \tag{1}$$

with

$$\langle\cos^2\varphi\rangle = \frac{\int_0^{2\pi} \mathrm{d}\varphi (I_q(\varphi)\cos^2(\varphi)|\sin(\varphi)|)}{\int_0^{2\pi} \mathrm{d}\varphi (I_q(\varphi)|\sin(\varphi)|)} \tag{2}$$

Depending on the type of alignment, two different ranges of the order parameter exist. For lamellar alignment parallel to the electrodes (maximum scattering intensity at $\varphi = 0°$), P_2 ranges from 0 to 1 with $P_2 = 1$ corresponding to perfect lamellar alignment parallel to the electrodes. For an alignment of the lamellae along the field direction (maximum scattering intensity at $\varphi = 90°$), P_2 ranges from 0 to −0.5 with $P_2 = -0.5$ corresponding to the fully oriented case. Full orientation, however, still allows for an isotropic distribution of the lamellae normals in the plane of the electrodes.

To quantify the orientation kinetics, the orientational order parameter P_2 was calculated for each single scattering pattern acquired during the course of the experiment. The behavior of P_2 as a function of time t could be fitted by a single exponential as described by

$$P_2(t) = P_{2,\infty} + (P_{2,0} - P_{2,\infty})\mathrm{e}^{-t/\tau} \tag{3}$$

with $P_{2,0}$ and $P_{2,\infty}$ being the limiting values of the order parameter before application of the electric field and at late times, respectively, and τ being the time constant.

Computer Simulation. We employ the dynamic density functional theory (DDFT), which describes the dynamic behavior of each molecule (modeled as Gaussian chains) in the mean field of all other molecules. This theory is a dynamic version of self-consistent-field theory for polymers.[24] The phase separation can be monitored by the scalar order parameter $\psi(\mathbf{r},t)$, which is the normalized deviation of the density of a polymer component from its average value. In the case of an incompressible diblock copolymer melt the system is described by only a single order parameter. Simulating a diblock copolymer solution requires an extra order parameter for the solvent; however, we use a simplified model with only one order parameter in the present study. It was shown theoretically that a block copolymer melt can serve as a good approximation to describe general features of phase behavior of concentrated block copolymers solutions with nonselective good solvents.[25] As we have shown recently, such a description is well justified and gives an excellent agreement with experiments in the case of a nonselective or almost nonselective

solvent.[26] The time evolution of the order parameter in the simplest case follows a diffusion-type equation[27]

$$\dot{\psi} = M\nabla^2\mu + \eta \tag{4}$$

with the constant mobility M, the thermal noise η, and a proper choice of the boundary conditions.[24] The chemical potential in the presence of an electric field $\mathbf{E}$ has the form $\mu = \mu^0 - (\partial\epsilon/\partial\psi)_T E^2/8\pi$,[28] where μ^0 is the chemical potential in the absence of the electric field, and ϵ is the dielectric constant of the polymeric material, which can be approximated as $\epsilon \approx \epsilon_0 + \epsilon_1\psi$ for small ψ. The electric field inside the material $\mathbf{E}$ deviates from the applied electric field $\mathbf{E}_0 = (0,0,E_0)$, satisfying the Maxwell equation div $\epsilon\mathbf{E} = 0$, where $\mathbf{E} = \mathbf{E}_0 - \nabla\varphi$. Keeping only leading terms, one can rewrite eq 4 in the form[21]

$$\dot{\psi} = M\nabla^2\mu^0 + \alpha\nabla_z^2\psi + \eta, \quad \alpha \equiv ME_0^2\frac{\epsilon_1^2}{4\pi\epsilon_0} \tag{5}$$

The chemical potential without the electrostatic contribution μ^0 is calculated using self-consistent-field theory for the ideal Gaussian chains with the mean field interactions between copolymer blocks A and B, described by a parameter ϵ_{AB}.[24]

The model system we study in the following is a symmetric A_4B_4 copolymer melt with mean field interactions $\epsilon_{AB} = 6$ kJ/mol. The simulations have been performed in two dimensions. In our previous work,[21] the behavior of this system was found to be drastically different from the system farther from ODT with $\epsilon_{AB} = 8$ kJ/mol. For the simulations, the electric field strength is parametrized by $\tilde{\alpha} \equiv \alpha/kTMv$.[21]

Results and Discussion

Structure Formation in the Absence of an Electric Field. Before we discuss the effects of external electric fields on the PS-*b*-PI block copolymer domains, we first concentrate on the microdomain structure formed in solution in the absence of an electric field. Toluene was chosen as solvent as it is fairly nonselective for PS and PI.[29,30] The Flory−Huggins interaction parameters between the polymers and toluene at room temperature are $\chi_{PS/Tol} = 0.44$ and $\chi_{PI/Tol} = 0.40$.[29−31] As anticipated from previous investigations on concentrated solutions of symmetric PS-*b*-PI block copolymers in toluene,[32] we observe the evolution of a lamellar microstructure with increasing concentration, as shown in Figure 2A. Above a polymer concentration of $w_p = 34$ wt %, the system exhibits higher order Bragg peaks appearing at integer multiples of the first-order maximum. The lamellar spacing $d = 2\pi/q^*$ was determined from the first-order scattering maxima. It was found to grow with increasing polymer concentration, indicating a stronger segregation power (or growing repulsive interactions) between the PS and PI chains as the polymer concentration increases (Figure 2B).

The appearance of higher order Bragg peaks, and their significant sharpening was used to locate the order−disorder transition (w_{ODT}) at room temperature at a polymer concentration $w_{p,ODT} = 34.5 \pm 1.0$ wt %. This assignment is corroborated by the absence of birefringence at and below $w_p = 34$ wt %, which shows the absence of randomly oriented lamellae.[33−35] Additional evidence is given by the fact that only for concentrations greater than 34 wt % we observe an anisotropic scattering pattern, which indicates some microdomain alignment induced either by shear (during the filling of the sample chamber) or by preferential attraction of one block to the electrode surface. We note that the peak in the scattering profile for $w_p \leq 34$ wt %

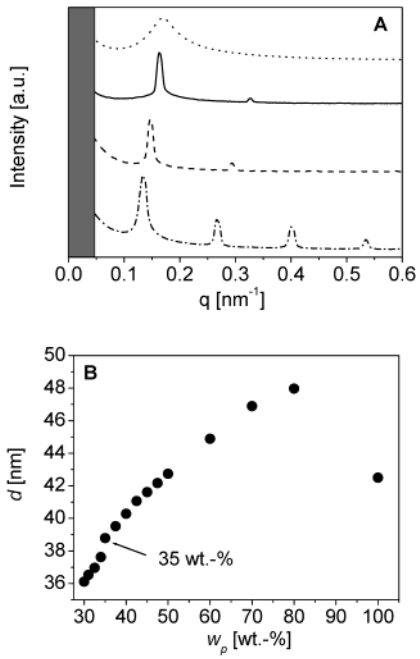

Figure 2. (A) Scattering intensity profiles at various concentrations: 34 wt % (· · ·), 35 wt % (—), 50 wt % (- - -), 70 wt % (- · -). (B) Concentration dependence of the lamellar spacing of PS-*b*-PI solutions in toluene ($d_{bulk} = 42.5$ nm).

is due to composition fluctuations commonly found in the disordered state (correlation hole).

At this point, we may compare our result on $w_{p,ODT}$ to earlier measurements on similar systems (SI in toluene solution). Yao et al. determined $w_{p,ODT}$ of a symmetrical PS-*b*-PI block copolymer ($M_w = 84\,000$ g/mol) in toluene solution by dielectric measurements and found a critical concentration between 25 and 28 wt % at 273 K.[36] As our measurements have been conducted at room temperature (∼298 K), it is reasonable that we find a slightly higher concentration. Sakamoto et al. determined $w_{p,ODT}$ for a symmetrical SI block copolymer of higher molecular weight to be around 22 wt % and estimated $w_{p,ODT}$ for the Yao system to be around 31 wt % at room temperature.[37] Both results compare well with our findings.

We note that the melt lamellar spacing found after solvent evaporation ($w_p = 100\%$ in Figure 2B) appears to be significantly smaller than what would be expected by extrapolation of the solution data. This observation indicates the formation of a nonequilibrium structure during the solvent-casting process. As the concentration of the solution increases, the glass transition temperature T_g reaches room temperature and the viscosity of the solution grows significantly. This augmentation of the overall modulus leads to a prolonged equilibration time for the deformation of grains, i.e., the displacement of the chemical junction points of the blocks, which is required for an increase in domain spacing, is hindered. This "frozen" domain structure is incapable of reaching an equilibrium at time scales smaller than the rate of solvent evaporation. Therefore, further solvent evaporation results in a decrease of the spacing merely by a *deswelling* effect. Thus, in the high concentration regime the domain spacing is kinetically, but not thermodynamically, controlled.

Reorientation Behavior of PS-*b*-PI in Toluene. Before we apply the electric field, all samples exhibit a distinctly anisotropic scattering pattern with maxima

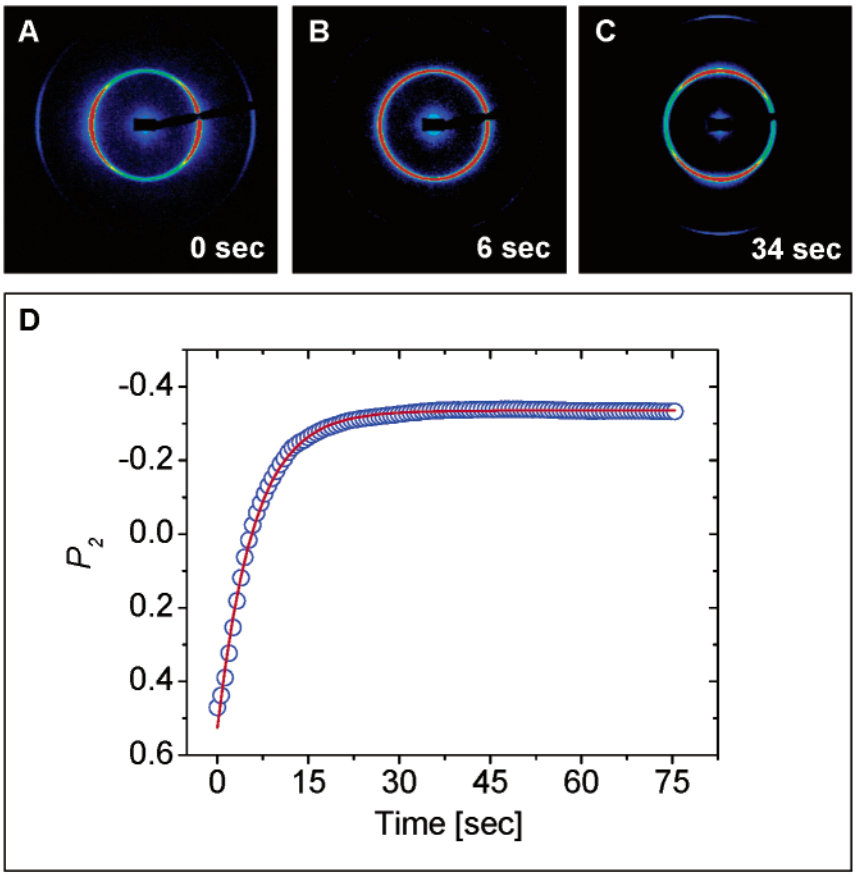

Figure 3. (A−C) Two-dimensional SAXS patterns of a 35 wt % solution of the SI-80 diblock copolymer in toluene taken at room temperature prior (A) and after (B, C) application of an electric field (E = 1 kV/mm). (D) Time dependence of the orientational order parameter P_2. The solid line is a least-squares fit to the data according to eq 3 with $P_{2,0} = 0.52$, $P_{2,\infty} = -0.32$, and $\tau = 5$ s.

located at $\varphi = 0°$ and 180° (Figure 3A). This finding indicates an alignment of the lamellae parallel to the electrodes. Such an alignment can be caused both by preferential interaction of the PS with the Au surfaces[3] and by possible shear forces acting on the highly viscous solutions during the filling of the capacitor with a syringe. To destroy any possible memory effect, we heated the solutions above the order−disorder temperature. However, after cooling, still some alignment of the domains parallel to the electrodes prevailed, revealing the importance of the surface effects.

As soon as the electric field is applied (Figure 3B,C), the scattering pattern changes significantly. The peaks at $\varphi = 0°$ and 180° decrease, and new scattering maxima at $\varphi = 90°$ and 270° grow with time (Figure 5A). To quantify the kinetics of the orientation process, the orientational order parameter $P_2(t)$ was calculated from the 2D SAXS images as outlined above. Using a single-exponential fit, we can determine the time constant of the reorientation process (Figure 3D).

Kinetics of Microphase Orientation. For the effective preparation of highly anisotropic melt block copolymer samples via solvent casting in the presence of an external electric field, it is important to find an optimum set of parameters (e.g., degree of swelling of the block copolymer domains, electric field strength, and temperature), which combines a maximum chain mobility (i.e., fast kinetics) with the highest possible polymer concentration. In short, the reorientation process should be faster than the rate of solvent evaporation during preparation of bulk samples from solution; i.e., it should be completed before the bulk structure "freezes".

Concentration Dependence. In a first series of experiments, we studied the reorientation kinetics as a function of polymer concentration, starting from w_p = 30 wt % and increasing w_p stepwise by 1 wt % up to 35 wt % and then by steps of 2.5 wt % to higher polymer concentrations. The electric field strength E was kept constant at E = 1 kV/mm at a capacitor spacing of 2 mm. The isotropic scattering pattern observed at polymer concentrations at and below w_p = 34 wt % did not change in the presence of the electric field. Above w_p = 34 wt %, the scattering patterns changed similar to the behavior shown in Figure 3 so that time constants $\tau(w_p)$ could be determined from the time evolution of P_2, as shown in Figure 4. Above w_p = 50 wt %, however, the reorientation process was so slow ($\tau \approx 5$ min) so that we limited our study to polymer concentrations between 34.5 and 50 wt %.

The results of the exponential fits and the increase of the time constant τ with increasing polymer concentration are summarized in Table 1. The single-exponential fit works quite well for all concentrations studied, as can be seen from the low χ^2 values. The time constants vary from $\tau = 0.8$ s for the very fast processes at 34.5 wt % to more than 3 min (τ = 192 s) for the 50 wt % solution. In addition, within some 10% scatter P_2 reaches about the same limiting values $P_{2,\infty} = -0.3 \pm 0.03$ independent of polymer concentration. Therefore, we can conclude that the polymer concentration only influences the rate but not the final degree of orientation. We note that the behavior displayed in Figure 4 results from a delicate balance between an increase of both the driving force for reorientation (i.e., a larger

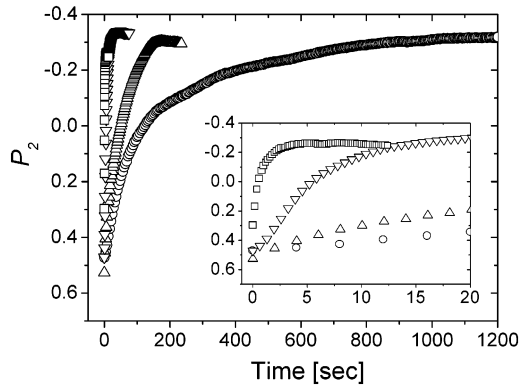

Figure 4. Evolution of the orientational order parameter P_2 with time for different concentrations at 2 kV/2 mm (□, 34.5 wt %; ▽, 37.5 wt %; △, 42.5 wt %; ○, 50 wt %).

Table 1. Time Constants τ of the Reorientation Behavior at Different Polymer Concentrations Obtained from Least-Squares Fits Using Eq 3 (E = 2 kV/2 mm); in Addition, the Rotational Time Constant, τ_{rot}, Was Determined Following the Procedure Published Previously[20] (NG = Nucleation and Growth, R = Rotation of Lamellae)

w_p [wt %]	τ [s]	τ_{rot} [s][20]	$P_{2,\infty}$	χ^2 [10^{-4}]	dominating mechanism
34.5	0.8		−0.26	0.6	NG
35	5.0	3.3	−0.32	1.4	NG
37.5	7.0	5.1	−0.34	0.8	NG
40	28.3	14.7	−0.33	1.3	NG
42.5	54	20	−0.33	2.4	mixed
45	104	40	−0.34	3.2	R
47.5	142	82	−0.26	1.2	R
50	192	170	−0.31	5.6	R

dielectric contrast) and the viscous drag as the polymer concentration is increased.[20] The exact behavior is difficult to predict; however, the data shown in Figure 4 and Table 1 indicate that in the particular system studied here the increase in viscosity dominates over the increase of the driving force. Therefore, the reorientation process slows down with increasing polymer concentration.

Interestingly, along with an overall slowing down of the reorientation at higher polymer concentration, the microscopic mechanism of microdomain reorientation changes as a function of the polymer concentration. This can be seen in Figure 5, where we compare the time dependence of the scattering patterns for the limiting polymer concentrations, w_p = 35 and 50 wt %. For the lower concentration (Figure 5A) the initial peaks at φ = 0° and 180° vanish almost completely (which is accompanied by a temporary drop in the normalized relative integrated intensity, Figure 5C) as the electric field is applied. New peaks establish at the final microdomain orientation at φ = 90° and 270°, showing a continuous growth of intensity with time. Intermediate orientations are not observed. For high polymer concentrations (Figure 5B) a distinctly different behavior is found. The initial peaks continuously shift from their original positions to their final positions at φ = 90° and 270°, respectively. The relative integrated intensity of the peaks increases steadily during the shift (Figure 5D); i.e., a well-defined anisotropic scattering pattern is observed throughout the entire process. At intermediate concentrations (not shown here) both behaviors coexist. Table 1 shows the prevailing mechanism found for the respective concentration.

Table 2. Time Constants of the Reorientation Behavior at Different Temperatures Obtained from Least-Squares Fits Using Eq 3 (w_p = 47.5 wt %, E = 2 kV/2 mm) (NG = Nucleation and Growth, R = Rotation of Lamellae)

temp [K]	τ [s]	$P_{2,\infty}$	χ^2 [10^{-4}]	dominating mechanism
300.15	141	−0.34	4	R
308.15	138	−0.28	0.6	R
316.15	106.9	−0.27	3	R
324.65	86.5	−0.28	3.8	mixed
333.65	52.5	−0.28	2.3	mixed
343.15	40.6	−0.27	2.5	NG
353.15	11.5	−0.25	0.2	NG

Temperature Dependence. A qualitatively similar behavior is found when we follow the reorientation process at different temperatures. For this purpose, a 47.5 wt % solution was studied between 27.3 and 80 °C. The rather high polymer concentration was chosen to access a large temperature range before reaching the order−disorder transition temperature (T_{ODT}) of the solution. Qualitatively, we find a "rotation" of the scattering pattern from the initial to the final situation at low temperatures, while the scattering pattern "switches" between the two limiting situations at temperatures near T_{ODT}. The results of a quantitative data evaluation are summarized in Table 2. At the lowest temperature (27 °C) we measure a time constant of 141 s, which gradually decreases down to 11.5 s as the temperature is raised to 80 °C. The plateau values of the orientational order parameter $P_{2,\infty}$ seem to show a slight increase from −0.34 to −0.25 with increasing temperature, indicating a decrease of order.

Mechanism of Domain Alignment. One of the most important aspects for the understanding of the reorientation behavior of block copolymer microdomains in solution is the knowledge of the underlying mechanisms contributing to the rearrangement of domains. In contrast to in-situ birefringence,[7,38] in-situ SANS,[35,39] and ex-situ SAXS[40−42] measurements on block copolymer melts and solutions under shear, which lead to detailed insight into the respective mechanisms, so far only little is known about the microscopic processes during electric field alignment. Synchrotron SAXS combines the advantages of birefringence (high time resolution) with the detailed and straightforward information about the microscopic order characteristic of scattering methods. Indeed, the SAXS data indicate two distinctly different mechanisms of microdomain reorientation. At low concentrations and at high temperatures, a destruction of the initial peaks is followed by a buildup of scattering intensity at the final peak positions. At high concentrations and low temperatures, on the other hand, the scattering pattern merely shifts into new peak positions accompanied by a steady increase in integrated peak intensities.

These findings point to two different underlying mechanisms responsible for microdomain reorientation in the presence of the electric field. Close to the order/disorder transition (ODT), i.e., at low concentrations and high temperatures, microdomains aligned parallel to the electric field grow at the expense of those aligned parallel to the electrodes. Intermediate orientations, however, are not observed. This behavior matches the notion of the migration of grain boundaries, which has previously been described for microdomain alignment under shear[41] and which was assumed to play a role in earlier electric field experiments.[11,12] In this case one lamella grows at the expense of another with a signifi-

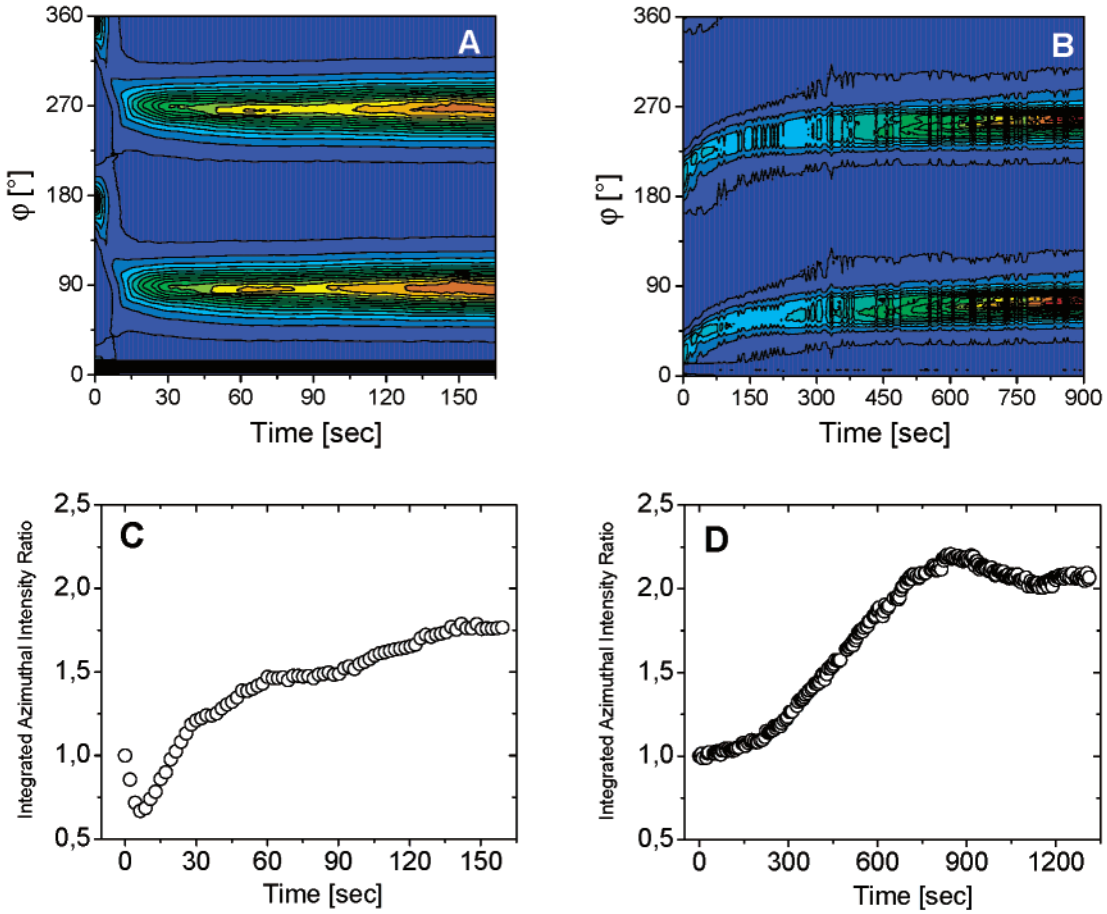

Figure 5. Azimuthal angular dependence of the scattering intensity and normalized relative integrated scattering intensity for different concentrations at 2 kV/2 mm. (A, C) 35 wt %, (B, D) 50 wt %.

cantly different orientation by motion of a tilt boundary (wall defect) between them, leading to a direct transfer of scattering intensity between widely separated azimuthal angles φ. This is indeed observed in Figure 5A. The integrated scattering intensity (as shown in Figure 5C) exhibits a temporary drop to 65% of the initial intensity, which coincides with the decrease of the peaks of the initial orientation, indicating the formation of an intermediate structure, e.g., nucleation centers for lamellar grains oriented parallel to the electric field. Their subsequent growth finally leads to an increase of the integrated intensity at later stages of the process.

Further away from the ODT, i.e., for high concentrations and low temperatures, the scattering pattern seems to be preserved and merely rotates into the new orientation. This observation points to the rotation of entire grains as an alternative orientation process. In contrast to the migration of grain boundaries, microdomain orientations intermediate between the original and the final orientations are observed. At the same time no increase in isotropic scattering intensity is found. We note that, in contrast to the migration of grain boundaries, the integrated scattering intensity in Figure 5B is found to grow continuously (Figure 5D). This indicates an overall growth of domains in the course of the reorientation process. In contrast to mechanical shear fields, the electric field does not impose a preferred direction of domain rotation on the system. The fact that the final orientation parallel to the electric field vector is not fully reached within the experimental time frame is in agreement with the notion that the driving force for grain alignment almost vanishes as the aligned state is approached.[12]

The transition from grain rotation to migration of grain boundaries can be explained by the fact that close to ODT we expect concentration fluctuations which can be amplified using an external electric field; i.e., the lamellar structure can easily be distorted in the direction of the electric field vector. In addition, the mobility of defects such as wall defects at the grain boundaries is much higher.

To further verify the above notion and to gain a more detailed understanding of the governing reorientation mechanisms, two-dimensional dynamic density functional theory simulations have been performed on lamellar block copolymer melts, which were able to reproduce the time evolution of the scattering pattern observed in the experiments.[21] The scattering functions calculated from these simulations are shown in Figure 6 and exhibit the same characteristic features seen in the experimental scattering intensity in Figure 5. These simulations are based on energetic considerations namely involving electrostatic (i.e., driving force of the process) and interfacial energy (i.e., incompatibility between the block copolymer domains) arguments. In Figure 7, we show a typical area of a large simulation box cropped around a newly forming grain for a system close to the ODT ($\epsilon_{AB} = 6$ kJ/mol) at an electric field strengths $\tilde{\alpha} = 0.2$. The initial structure ($t = 5.0$) has first been aligned parallel to the electrodes by shear. Immediately after the application of the electric field (at $t = 5.1$), the lamellae become unstable and exhibit undulations very

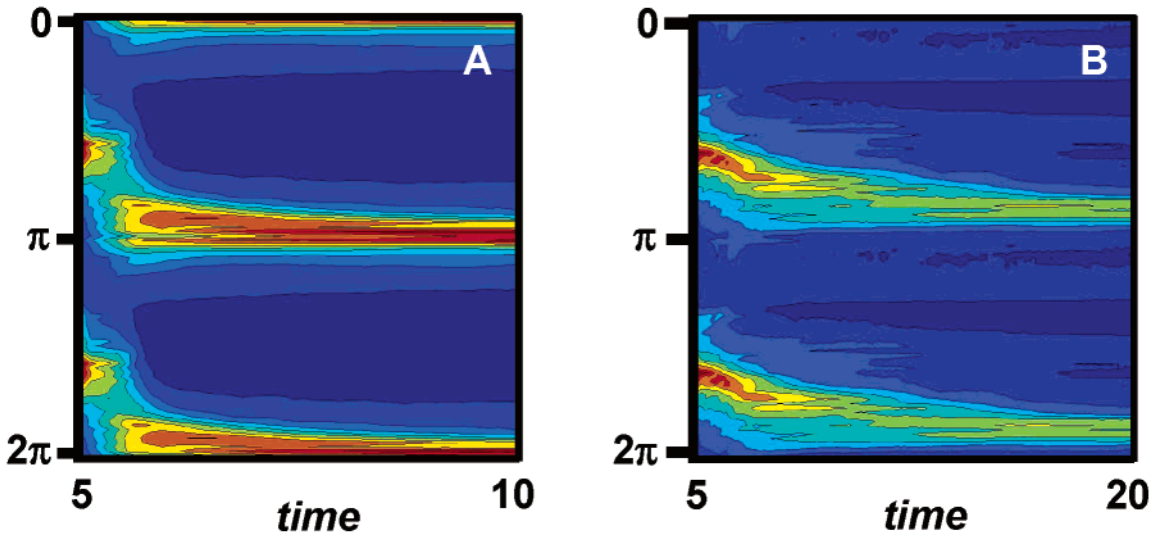

Figure 6. Fourier transform squared as obtained by dynamic density functional theory (MesoDyn)—simulation of lamellar reorientation at dimensionless time t (in units of 10^3). (A) $\epsilon_{AB} = 6$ kJ/mol, (B) $\epsilon_{AB} = 8$ kJ/mol.

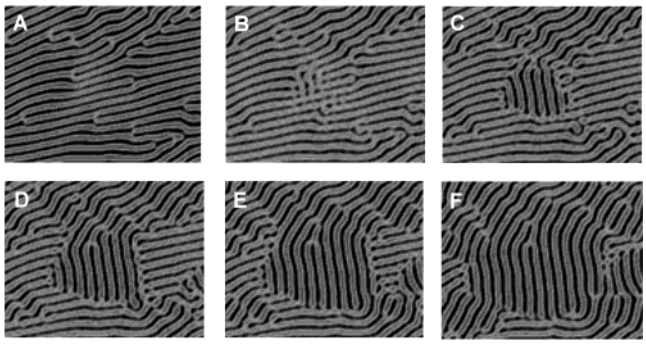

Figure 7. Dynamic density functional theory (MesoDyn)—simulation of reorientation close to ODT ($\epsilon_{AB} = 6$ kJ/mol) at dimensionless time t (in units of 10^3). (A) 5.0, (B) 5.1, (C) 5.2, (D) 5.3, (E) 5.4, (F) 5.5. The electric field vector runs vertically. Alignment by nucleation and growth and grain rotation can be distinguished.

similar to the ones described by Onuki and Fukuda[43] and, eventually, form pointlike defects. Those serve as nucleation centers for grains with lamellar orientation parallel to the electric field. As the process evolves, new instabilities are formed around the new structure contributing to the growth of the grain with lamellar orientation parallel to the electric field at the expense of all other orientations. Interestingly, the grain seems to grow faster in the direction perpendicular to the electric field vector. On the other hand, the lower left corner of the simulation box shows a different mechanism. Here, the reorientation, initiated by undulations, proceeds via movement of defects (disclination lines) and merely results in a rotation of the lamellar structure. This finding supports our previous notion that the two distinct mechanisms can be simultaneously found in our system. Depending on the degree of phase separation one of the two is dominant. In the presented simulation, as can be seen clearly also from the larger simulation boxes, the *nucleation and growth* mechanism prevails.[21] For simulations further away from ODT, we predominantly find that the *rotation of grains* mechanism (induced by the movement of well-defined defects) governs the reorientation process. The governing mechanisms can be identified clearly from the squared Fourier transforms of the simulated lamellar rearrangement as depicted in Figure 6A,B,[21] which closely resembles the experimental data shown in Figure 5A,B. Obviously, for the systems further away from ODT, the energetic cost for additional creation of defects as required for the nucleation and growth process is too high compared to the gain in energy from an aligned lamellar phase.

We are well aware of the limits of the simulation approach, which does not include changes in the kinetics of the system as the degree of incompatibility is changing. Still, the simulations reveal results that are strikingly similar to the experimental findings, thereby supporting the idea of two different microscopic processes determining the reorientation process close to and far from ODT.

Our mechanistic model is further corroborated by typical structural defects, so-called "kink bands" (Figure 8D), which are characteristic of the above-described mechanisms and have been identified in similar processes during shear-induced lamellar reorientation.[41] Figure 8E shows the annihilation of a kink band by rotation of the defect structure. Also, computer simulations show that "kink bands" are one of the typical defects that form when the structure reorients (Figure 10C).

Electric Field Dependence. Earlier studies on thin film melt samples have revealed the existence of a threshold value of the electric field strength, below which no reorientation was observed.[16] The authors rationalized this finding by the competing effects of the surfaces (favoring orientation parallel to the capacitor plates) and the electric field (favoring orientation perpendicular to the capacitor plates). Theoretical investigations have verified this model.[44] To investigate the influence of the electric field strength on the orientation behavior in the block copolymer solutions studied here, we varied the electric field between $E = 0.25$ kV/mm and $E = 3$ kV/mm. Again, a 35 wt % solution was studied at room temperature in a capacitor with 2 mm electrode spacing. Quite similar to the studies referred to above, we find an electric field induced reorientation only at and above an electric field strength of $E \geq 0.375$ kV/mm. At lower electric fields ($E \leq 0.25$ kV/mm) no influence of the electric field was observed (Figure 9B).

One has to realize, though, that whether a field-induced reorientation is observed may well depend on

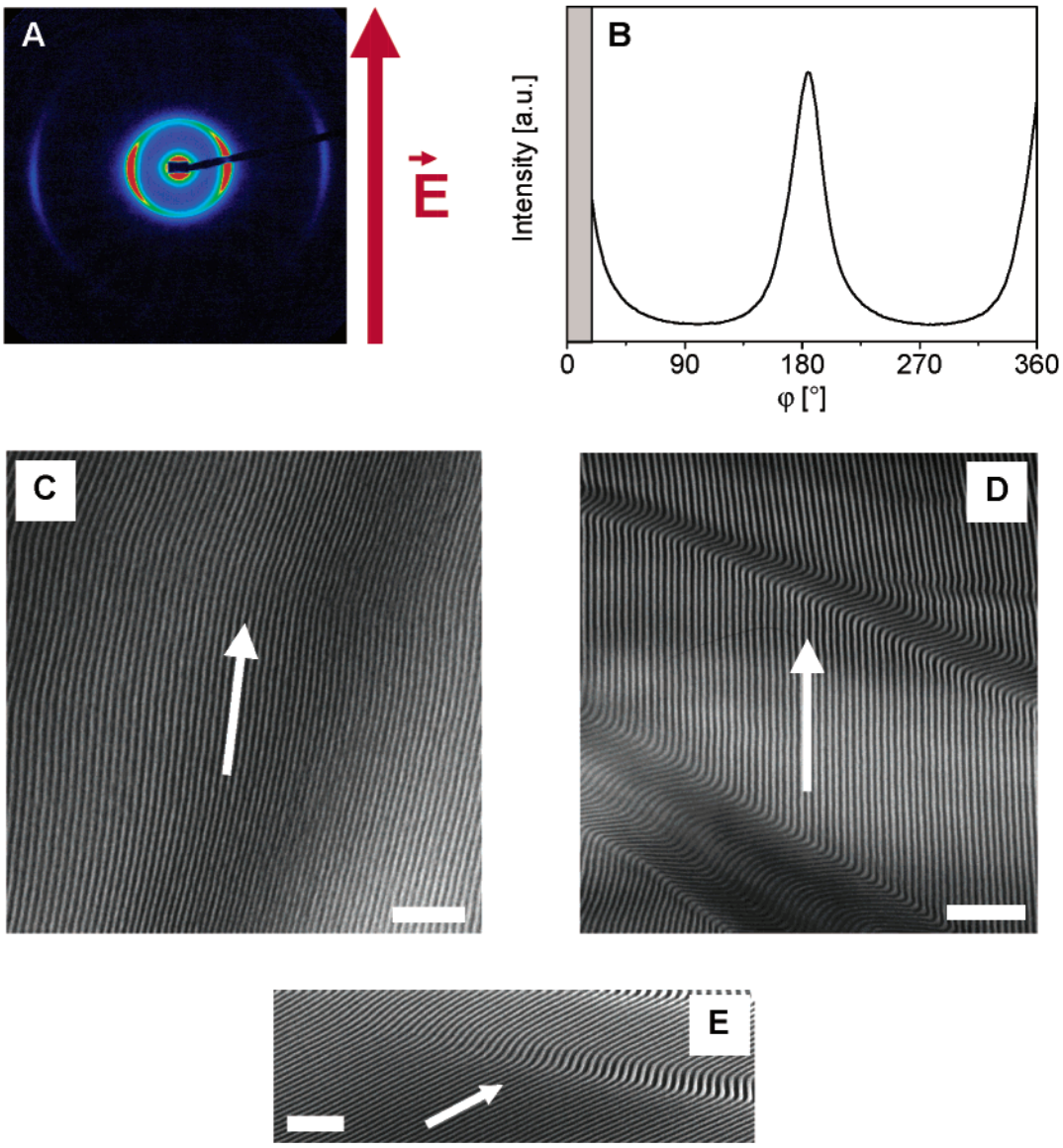

Figure 8. SAXS and TEM data of a bulk sample prepared from a 40 wt % solution of SI-80 in toluene dried under an applied electric field of 1 kV/mm. The arrows indicate the direction of the electric field vector. (A) 2D SAXS pattern and (B) azimuthal intensity distribution at first-order reflection ($P_2 = -0.34$). The TEM pictures show a defect free domain (C) and characteristic kink band defects (D/E). The scale bars represent 400 nm.

the time scale of the experiment. Indeed, if we monitor the reorientation kinetics in detail (Figure 9A), we find that the process is slowed down significantly if the electric field strength is decreased. In consequence, the time needed to achieve any measurable change in the scattering pattern will increase with decreasing field strength as well. Therefore, both in the melt experiments and in the experiments reported here, the exact value of the threshold electric field will to some extent depend on the time allowed for reorientation. From our kinetic experiments we can define a threshold electric field strength as the value of the electric field at which the time constant for reorientation diverges.

The results on the reorientation kinetics are shown in Figure 9 and summarized in Table 3. The quality of the single-exponential fits can be inferred from the low χ^2 values. Independent of the electric field strength, the limiting values $P_{2,\infty}$ always reach a value around $P_{2,\infty} = -0.3$ within a scatter of some 10%. The time constants τ range from 100 s for low electric fields (0.375 kV/mm) to as low as 0.34 s for the highest field strength (3 kV/mm). The dependence of the time constant on the electric field reveals a power law dependence $\tau = \alpha(E - E_t)^a + \tau_\infty$. The data points are best fitted for $\alpha = 0.2$ s, $a = -1$, $E_t = 350$ V/mm, and $\tau_\infty = 0$ s (solid line in Figure 9B). Obviously, the error in determining the threshold electric field E_t is rather large because of the limited number of data points at low field strength.

Qualitatively, the same effect is revealed by the computer simulations (Figure 10). Starting from parallel alignment of the domains before application of the electric field (Figure 10A), a different response is found for different field strengths (expressed in the parameter $\tilde{\alpha}$).[21] For the highest value of $\tilde{\alpha}$ (Figure 10D), almost perfect reorientation is found after the electric field was applied for a time $t = 10$. For lower field strength ($\tilde{\alpha} = 0.1$) (Figure 10C), only the onset of reorientation is observed after the electric field was applied for the same time. Finally, at the lowest value of $\tilde{\alpha}$ ($\tilde{\alpha} = 0.05$) (Figure 10B), no signs of reorientation can be found at all until the end of the simulation at $t = 10$. Although

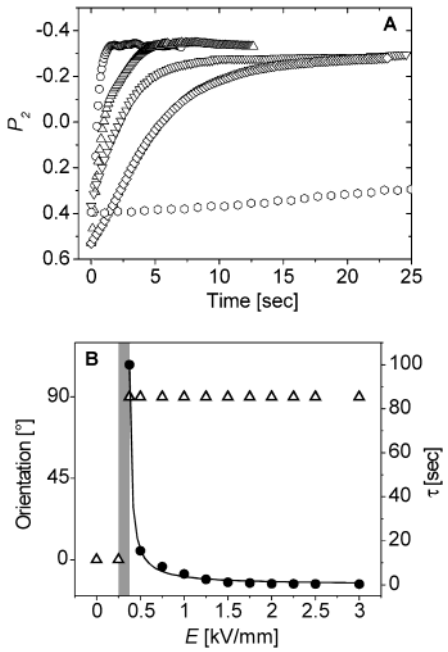

Figure 9. (A) Evolution of the orientational order parameter P_2 with time for 35 wt % solutions at different field strengths (○, 375 V/mm; ◊, 1 kV/mm; ▽, 1.25 kV/mm; △, 1.5 kV/mm; ○, 3 kV/mm; electrode spacing: 2 mm). (B) The achieved orientation at the respective field strength is represented by open triangles (0°: alignment parallel to the electrodes; 90°: alignment parallel to the electric field vector). The filled circles show the electric field dependence of the time constant, τ. The solid line represents a least-squares fit of the power law $\tau = \alpha(E - E_t)^a + \tau_\infty$ to the data points.

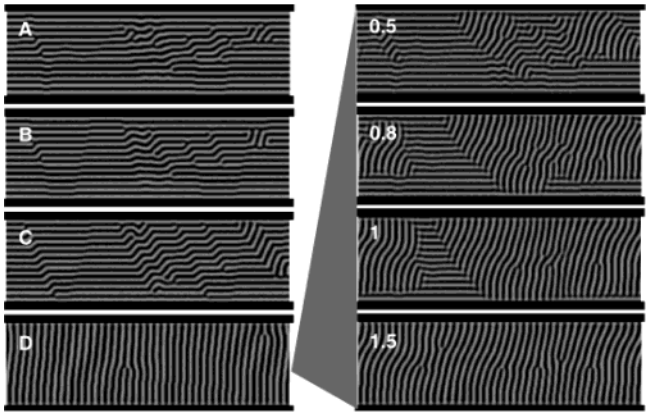

Figure 10. Indication for the existence of a threshold electric field strength from MesoDyn simulations. Starting from parallel alignment prior to application of the electric field (A), the microdomain structure has been captured at later times for three different values of the electric field strength. At the highest value ($\tilde{\alpha} = 0.2$) almost perfect alignment is achieved after the electric field was applied for the time $t = 10$ (D). For lower field strength hardly any ($\tilde{\alpha} = 0.1$) and no effect at all ($\tilde{\alpha} = 0.05$) is observed after the electric field was applied for the same time (C, B). One of the blocks is preferably attracted by the electrodes ($\epsilon_{AM} = 7.5$ kJ/mol, $\epsilon_{BM} = 0$ kJ/mol in notations of ref 21). On the right-hand side the early stages of the reorientation process of (D) are shown (time t given in upper left corner). The simulation reveals migration of grain boundaries and rotation of lamellae by movement of defects.

the system size is rather small (thus, highly exaggerating the effects of the surfaces), the results agree quite well with the experimental finding. In addition, we note that the simulation again reveals the migration of grain boundaries accompanied by the rotation of lamellae induced by defect movement as the two mechanisms

Table 3. Time Constants of the Reorientation Behavior at Different Electric Field Strength Obtained from Least-Squares Fits Using Eq 3 ($w_p = 35$ wt %, Electrode Spacing: 2 mm)

voltage [kV/mm]	τ [s]	$P_{2,\infty}$	χ^2 [10^{-4}]
0.25	*a*	*a*	*a*
0.375	100.1	−0.26	4.3
0.5	15.5	−0.32	2.3
0.75	8.3	−0.31	0.4
1	5.0	−0.32	1.4
1.25	2.5	−0.29	0.3
1.5	1.2	−0.34	1.8
1.75	0.90	−0.32	1.5
2	0.56	−0.29	4.2
2.25	0.48	−0.33	4
2.5	0.40	−0.35	3.8
3	0.34	−0.34	3.7

[a] No electric-field-induced reorientation observed on the time scale of experiment.

leading to reorientation of the microdomain structure (Figure 10, right-hand side).

Dried Bulk Samples. Finally, we return to the preparation of anisotropic bulk samples by the alignment-during-drying method. Our kinetic measurements have shown that all concentrations up to 50 wt % can in principle be used for this method as for this concentration we find a time constant of 192 s with the overall orientation process being finished within 20 min. As has been described earlier, even this process should be faster than the rate of solvent evaporation.

Using a home-built capacitor which allows the application of a dc electric field during film formation by solvent casting,[19] we have demonstrated the feasibility of such a process. This can be seen from the SAXS and TEM data of the resulting melt sample prepared from a 40 wt % solution dried under an applied electric field of 1 kV/mm (Figure 8A−C).

Nevertheless, in all our experiments, we did not find degrees of orientation described by P_2 values lower than −0.35 for the block copolymer solutions and the melt sample, which are still significantly larger than the expected value for perfect alignment parallel to the electric field vector ($P_2 = -0.5$). In the following, we will consider several possible explanations for these observations. First we have identified the movement of defects at grain boundaries, so-called wall defects, as the main mechanism in samples close to ODT. It has been shown for electric field alignment of melt samples that other defects like disclination lines can reduce the mobility of grain boundaries significantly as the movement of a wall defect along a disclination line is associated with an energetic penalty which can even lead to final pinning of the boundary.[11,17] This eventually leads to the clustering of defects. Generally, the electric-field-induced force on these clusters at field strengths used in this work is not sufficient to favor further defect annihilation. Moreover, the rotation of whole grains must be associated with a large-scale reformation of the lamellar structure, thus creating new defects. In addition, the electrodynamic driving force scales with $\cos^2 \theta$, where θ is the tilt angle of the lamellar normal vector with respect to the electric field vector. This results in a reduction of the driving force to as low as 3% for lamellae slightly misaligned by 10° from a perfect orientation parallel to the electric field. In all cases, the application of higher electric fields than have been accessible in this work could improve the degree of alignment.

Conclusion

We have identified two mechanisms governing the electric field alignment of a lamellar block copolymer from concentrated solutions. It was shown that depending on the segregation power ($\chi \propto \phi_P$, $\chi \propto 1/T$) a single mechanism dominates the orientation process. In a weakly segregated system (low concentration or high temperature) nucleation and growth of new microdomains prevails, whereas a stronger phase-separated system (high concentration or low temperature) predominantly exhibits rotation of grains. Dynamic density functional theory computer simulations corroborate these experimental findings.

Additionally, we determined the influence of the electric field strength on the orientation kinetics. We find a significant slowdown of the reorientation process on decreasing electric field strength, which eventually leads to a threshold value below which no electric field induced orientation can be achieved on the time scale of the experiment. The time constants of the fastest processes were in the range of 0.5 s, reaching a final orientation described by order parameters of down to $P_2 = -0.35$. Finally, the variation of temperature enables us to control the governing mechanisms at a fixed polymer concentration.

In summary, we have demonstrated that electric field alignment of block copolymer domains from solution is a powerful tool to generate highly anisotropic bulk block copolymer samples. The variety of parameters that are accessible in our experiments allows us to further improve the preparation of macroscopically aligned melt samples via solvent casting in the presence of an electric field.

Acknowledgment. The authors thank H. Krejtschi and his team for the skillful assistance in constructing the experimental setup. We are grateful for many helpful discussions with H. Brand. We thank A. Göpfert for the TEM measurements and H. Schmalz for the cooperation during the block copolymer synthesis. A.B. acknowledges a Kekulé fellowship by the Stiftung Stipendien-Fonds des Verbandes der Chemischen Industrie and the BMBF. We are grateful to the ESRF for financial support and provision of synchrotron beam time. This work was carried out in the framework of the Sonderforschungsbereich 481 funded by the Deutsche Forschungsgemeinschaft (DFG). In addition, we acknowledge support by the NWO (Nederlandse Organisatie voor Wetenschappelijk Onderzoek)-DFG bilateral program. Supercomputer time was provided by the NCF (Stichting Nationale Computerfaciliteiten).

References and Notes

(1) Bates, F. S.; Fredrickson, G. H. *Annu. Rev. Phys. Chem.* **1990**, *41*, 525.
(2) Bates, F. S.; Fredrickson, G. H. *Phys. Today* **1999**, *52*, 32.
(3) Anastasiadis, S. H.; Russell, T. P.; Satija, S. K.; Majkrzak, C. F. *Phys. Rev. Lett.* **1989**, *62*, 1852.
(4) Annighöfer, F.; Gronski, W. *Makromol. Chem., Rapid Commun.* **1983**, *4*, 123.
(5) Wiesner, U. *Macromol. Chem. Phys.* **1997**, *198*, 3319.
(6) Chen, Z.-R.; Kornfield, J. A.; Smith, S. D.; Grothaus, J. T.; Satkowski, M. M. *Science* **1997**, *277*, 1248.
(7) Chen, Z.-R.; Kornfield, J. A. *Polymer* **1998**, *39*, 4679.
(8) Keller, A.; Pedemonte, E.; Willmouth, F. M. *Nature (London)* **1970**, *225*, 538.
(9) Albalak, R. J.; Thomas, E. L. *J. Polym. Sci., Polym. Phys. Ed.* **1993**, *31*, 37.
(10) Thurn-Albrecht, T.; Schotter, J.; Kastle, G. A.; Emley, N.; Shibauchi, T.; Krusin-Elbaum, L.; Guarini, K.; Black, C. T.; Tuominen, M. T.; Russell, T. P. *Science* **2000**, *290*, 2126.
(11) Amundson, K.; Helfand, E.; Davis, D. D.; Quan, X.; Patel, S. S.; Smith, S. D. *Macromolecules* **1991**, *24*, 6546.
(12) Amundson, K.; Helfand, E.; Quan, X.; Smith, S. D. *Macromolecules* **1993**, *26*, 2698.
(13) Morkved, T. L.; Lu, M.; Urbas, A. M.; Ehrichs, E. E.; Jaeger, H. M.; Mansky, P.; Russell, T. P. *Science* **1996**, *273*, 931.
(14) Morkved, T. L.; Lopez, V. A.; Hahm, J.; Sibener, S. J.; Jaeger, H. M. *Polymer* **1998**, *39*, 3871.
(15) Mansky, P.; DeRouchey, J.; Russell, T. P.; Mays, J.; Pitsikalis, M.; Morkved, T. L.; Jaeger, H. M. *Macromolecules* **1998**, *31*, 4399.
(16) Thurn-Albrecht, T.; DeRouchey, J.; Russell, T. P.; Jaeger, H. M. *Macromolecules* **2000**, *33*, 3250.
(17) Amundson, K.; Helfand, E.; Quan, X.; Hudson, S. D.; Smith, S. D. *Macromolecules* **1994**, *27*, 6559.
(18) Le Meur, J.; Terrisse, J.; Schwab, C.; Goldzene, P. *J. Phys., Colloq.* **1971**, *32*, C5a-301.
(19) Böker, A.; Knoll, A.; Elbs, H.; Abetz, V.; Müller, A. H. E.; Krausch, G. *Macromolecules* **2002**, *35*, 1319.
(20) Böker, A.; Elbs, H.; Hänsel, H.; Knoll, A.; Ludwigs, S.; Zettl, H.; Urban, V.; Abetz, V.; Müller, A. H. E.; Krausch, G. *Phys. Rev. Lett.* **2002**, *89*, 135502.
(21) Zvelindovsky, A. V.; Sevink, G. J. A. *Phys. Rev. Lett.* **2003**, *90*, 049601.
(22) Schmalz, H.; Böker, A.; Lange, R.; Krausch, G.; Abetz, V. *Macromolecules* **2001**, *34*, 8720.
(23) Sawyer, C. C.; Grubb, D. T. *Polymer Microscopy*, 2nd ed.; Chapman & Hall: London, 1996.
(24) (a) Sevink, G. J. A.; Zvelindovsky, A. V.; van Vlimmeren, B. A. C.; Maurits, N. M.; Fraaije, J. G. E. M. *J. Chem. Phys.* **1999**, *110*, 2250. (b) van Vlimmeren, B. A. C.; Maurits, N. M.; Zvelindovsky, A. V.; Sevink, G. J. A.; Fraaije, J. G. E. M. *Macromolecules* **1999**, *32*, 646.
(25) Fredrickson, G. H.; Leibler, L. *Macromolecules* **1989**, *22*, 1238.
(26) Knoll, A.; Horvat, A.; Lyakhova, K. S.; Krausch, G.; Sevink, G. J. A.; Zvelindovsky, A.; Magerle, R. *Phys. Rev. Lett.* **2002**, *89*, 035501.
(27) Onuki, A. *Phase Transition Dynamics*; Cambridge University Press: New York, 2002.
(28) Landau, L. D.; Lifshitz, E. M. *Electrodynamics of Continuous Media*; Pergammon: Oxford, 1960; Chapter II.
(29) Huang, C.; Chapman, B. R.; Lodge, T. P.; Balsara, N. P. *Macromolecules* **1998**, *31*, 9384.
(30) Wang, W.; Hashimoto, T. *Polymer* **2000**, *41*, 4729.
(31) Noolandi, J.; Hong, K. M. *Ferroelectrics* **1980**, *30*, 117.
(32) Shibayama, M.; Hashimoto, T.; Hasegawa, H.; Kawai, H. *Macromolecules* **1983**, *16*, 1427.
(33) Amundson, K.; Helfand, E.; Patel, S. S.; Quan, X.; Smith, S. D. *Macromolecules* **1992**, *25*, 1953.
(34) Balsara, N. P.; Perahia, D.; Safinya, C. R.; Tirrell, M.; Lodge, T. P. *Macromolecules* **1992**, *25*, 3896.
(35) Balsara, N. P.; Hammouda, B.; Kesani, P. K.; Jonnalagadda, S. V.; Straty, G. C. *Macromolecules* **1994**, *27*, 2566.
(36) Yao, M. L.; Watanabe, H.; Adachi, K.; Kotaka, T. *Macromolecules* **1992**, *25*, 1699.
(37) Sakamoto, N.; Hashimoto, T.; Kido, R.; Adachi, K. *Macromolecules* **1996**, *29*, 8126.
(38) Chen, Z. R.; Issaian, A. M.; Kornfield, J. A.; Smith, S. D.; Grothaus, J. T.; Satkowski, M. M. *Macromolecules* **1997**, *30*, 7096.
(39) Balsara, N. P.; Hammouda, B. *Phys. Rev. Lett.* **1994**, *72*, 360.
(40) Winey, K. I.; Patel, S. S.; Larson, R. G.; Watanabe, H. *Macromolecules* **1993**, *26*, 2542.
(41) Polis, D. L.; Smith, S. D.; Terrill, N. J.; Ryan, A. J.; Morse, D. C.; Winey, K. I. *Macromolecules* **1999**, *32*, 4668.
(42) Zhang, Y.; Wiesner, U. *J. Chem. Phys.* **1995**, *103*, 4784.
(43) (a) Onuki, A.; Fukuda, J. *Macromolecules* **1995**, *28*, 8788. (b) Fukuda, J.; Onuki, A. *J. Phys. II* **1995**, *5*, 1107.
(44) Tsori, Y.; Andelman, D. *Macromolecules* **2002**, *35*, 5161.

MA021347K